AIAA JOURNAL
Vol. 45, No. 8, August 2007

Step Geometry and Countercurrent Effects in Dump Combustor, Part 1: Cold Flow

K. Sengupta,* K. Russell,* and F. Mashayek†
University of Illinois at Chicago, Chicago, Illinois 60607

DOI: 10.2514/1.28260

Nonreacting flow in a backward-facing step combustor is studied while employing a novel countercurrent shear (or counterflow) concept. Counterflow is used to manipulate the turbulent shear layer created by the step to increase turbulent burning velocities, and thereby, reduce ignition delay time. Unfortunately, this concept also leads to a smaller residence time because of a shorter recirculation vortex. These competing challenges of achieving higher burning velocities and longer residence time demand modification of the step geometry. Changes in the step geometry will alter the size and characteristics of the recirculation vortex and the shear layer dynamics within the combustor. These issues are addressed in this paper via a numerical study. For the simulations, Reynolds-averaged Navier–Stokes equations are solved in the framework of the realizable k–ϵ turbulence model. A two-layer approach is used for the near-wall modeling. The paper includes a detailed account of the benefits of countercurrent shear technology, a parametric study based on step-geometry modifications, and an aerodynamic performance evaluation.

Nomenclature

C_f	=	coefficient of skin friction drag on the bottom wall, $\tau_0/\frac{1}{2}\rho_0 U_0^2$
C_p	=	coefficient of pressure drag acting normal to the step wall, $(p - p_0)/\frac{1}{2}\rho_0 U_0^2$
G	=	suction gap height
H	=	step height of the combustor
k	=	turbulent kinetic energy
L	=	combustor length
L_r	=	length of the recirculation zone
P	=	production of turbulent kinetic energy
p	=	static pressure
p_0	=	reference pressure, atmospheric
S	=	strain rate
T	=	splitter plate thickness
$\bar{U}_i$	=	mean velocity in the ith coordinate direction
U_0	=	mean axial velocity at the inlet
U_1	=	maximum velocity of secondary stream
U_2	=	maximum velocity of primary stream
u_i'	=	turbulent fluctuation in ith coordinate direction
y_α	=	cross-stream location
δ	=	boundary-layer thickness
δ_{ij}	=	Kronecker delta
ϵ	=	turbulent dissipation
ρ_0	=	reference density, 1.225 kg/m^3
ν	=	molecular kinematic viscosity
ν_t	=	eddy viscosity (kinematic)
τ_{ij}	=	viscous stress tensor
τ_0	=	wall shear stress

I. Introduction

DUMP combustors are widely used in modern air breathing propulsion devices as an energy conversion component. A typical characteristic of a dump combustor is the sudden expansion of the flow downstream of a step or bluff body. The sudden expansion causes the flow to separate, leading to a low velocity recirculation zone that contains reacting mixture and serves as a continuous ignition source. Under ideal conditions, the incoming reactants should have sufficient residence time within the recirculation vortex to fully react. This reaction is needed to create hot combustion products, which would subsequently ignite the fresh reactants. A vast amount of research has been devoted to dump combustors with a rearward facing step. Investigations have often been focused on static pressure distributions, turbulence characteristics, and shear layer reattachment [1–4]. Many of the works were motivated by the drag characteristics of the separated boundary layer. A good portion of studies were also initiated to just document the base flow under isothermal conditions and different Reynolds numbers including direct numerical simulation works [5–7]. A thorough review of the findings for flow over a backward-facing step can be found in [8].

Countercurrent shear control has been successfully applied to free shear flows [9,10]. These flows, being essentially unconfined, have completely different dynamics compared with flows in dump combustors. Countercurrent shear flow that is applied to asymmetric step combustors was first investigated by Forliti [11]. The cold flow studies reported in this cited work indicated that high turbulence at a controlled strain rate could be generated by augmenting the naturally present counterflow within the combustor with additional suction. The overall benefits of a well-designed countercurrent dump combustor are a large increase in volumetric heat release rate and an extended stable operating condition.

Although the application of countercurrent shear technology to traditional step combustors has enormous cost benefits with regard to control of the turbulent flow field [11], this method may fail to provide adequate flame anchoring. A criterion based on two time scales for stabilizing a flame behind a bluff body was given by Frolov [12]. The two time scales considered in this theory are the ignition time (t_c) and residence time (t_r) in the turbulent mixing layer. The time needed for a fluid packet to be ignited in the mixing layer is referred to as the ignition time, whereas the residence time is defined as the time necessary to reach the turning point. The flame is stabilized when $t_c/t_r \leq 1$. Counterflow, through the manipulation of the turbulent shear layer created by the step increases turbulent burning velocities, and thereby, reduces ignition delay time. However, at the same time, it leads to a smaller residence time because of a shorter recirculation vortex. These competing challenges of achieving higher burning velocities and longer residence

Received 8 October 2006; revision received 14 March 2007; accepted for publication 23 March 2007.

*Graduate Student, Department of Mechanical and Industrial Engineering, 842 West Taylor Street.

†Professor, Department of Mechanical and Industrial Engineering, 842 West Taylor Street. Associate Fellow AIAA.

time demands modification of the step geometry. Changes in geometry will alter the size and characteristics of the recirculation vortex, affecting both turbulent energy production and flame anchoring performance.

In this work, we undertake a study of the nonreacting flow field within dump combustors with different step wall geometries and countercurrent shear. The goal is to select the best candidate geometry that would harness the benefits of the countercurrent shear and at the same time provide a suitable flame anchor. Such a geometry could prove to be very suitable for ramjet engines, where the current focus is to employ relatively simple, compact, and low-drag combustors with stable flame anchor. Ram compression in these engines leads to insufficient residence time for complete burning of typical hydrocarbon fuels. Countercurrent shear can potentially improve the overall burning efficiency by enhancing mixing and turbulence within the combustor. Experimental studies of reacting shear layers, both in unconfined [13,14] and confined [15–17] configurations, have demonstrated that the presence of heat release impacts the flow field, but qualitative features of the flow remain similar under reacting and nonreacting scenarios. Therefore, as a first step we investigate the effects of geometry change and counterflow under nonreacting conditions. The paper is organized as follows: First we briefly describe our computational tools and modeling approach. Then we investigate the effects of countercurrent shear in traditional step combustors. Next, studies on the effects of altering the step geometry are reported. The physical analysis is based on the parameters relevant to shear layer control, flame dynamics, and aerodynamic drag. Finally some concluding remarks are provided.

II. Numerical Modeling Approach

In our previous works [18–20], we have shown that Reynolds-average Navier–Stokes (RANS) modeling is a suitable technique for simulating two-phase reacting flow in practical configurations at an affordable computational time. Therefore, in this work we adopt the RANS approach for our analysis and design. A survey of existing literature [3,21–23] revealed that both two-equation based models and Reynolds stress closures have been used to simulate flows in backward-facing step configurations. Thus, to assess the viability of these models for the present problem, we tested the standard k–ϵ model, realizable k–ϵ model, and Reynolds stress model (RSM) against the experimental data of Forliti [11,24]. The results (which are discussed in the following section) demonstrate that the realizable k–ϵ model predicts the flow features fairly well. Thus, there is no need to resort to the arguably more accurate but, computationally expensive, full Reynolds stress closures. The complete set of equations for the realizable k–ϵ model is enumerated below,

$$\frac{\partial \bar{U}_i}{\partial x_i} = 0 \tag{1}$$

$$\frac{\partial \bar{U}_i}{\partial t} + \bar{U}_j \frac{\partial \bar{U}_i}{\partial x_j} = -\frac{1}{\rho}\frac{\partial p}{\partial x_i} + \frac{\partial \tau_{ij}}{\partial x_j} - \frac{\partial \overline{u_i' u_j'}}{\partial x_j} \tag{2}$$

$$\frac{\partial k}{\partial t} + \bar{U}_j \frac{\partial k}{\partial x_j} = \frac{\partial}{\partial x_j}\left[\left(\nu + \frac{\nu_t}{\sigma_k}\right)\frac{\partial k}{\partial x_j}\right] + P - \epsilon \tag{3}$$

$$\frac{\partial \epsilon}{\partial t} + \bar{U}_j \frac{\partial \epsilon}{\partial x_j} = \frac{\partial}{\partial x_j}\left[\left(\nu + \frac{\nu_t}{\sigma_\epsilon}\right)\frac{\partial \epsilon}{\partial x_j}\right] + C_1 S\epsilon - C_2 \frac{\epsilon^2}{k + \sqrt{\nu\epsilon}} \tag{4}$$

where the closure terms are described as

$$\overline{\tau_{ij}} = \nu\left(\frac{\partial \bar{U}_j}{\partial x_i} + \frac{\partial \bar{U}_i}{\partial x_j}\right); \qquad \overline{u_i' u_j'} - \frac{2}{3}k\delta_{ij} = \nu_t\left(\frac{\partial \bar{U}_j}{\partial x_i} + \frac{\partial \bar{U}_i}{\partial x_j}\right)$$
$$P = -\overline{u_i' u_j'}\frac{\partial \bar{U}_i}{\partial x_j} \tag{5}$$

and the eddy viscosity is computed as

$$\nu_t = C_\mu \frac{k^2}{\epsilon} \tag{6}$$

The values for the models constants are $C_{1\epsilon} = 1.44$, $C_2 = 1.9$, $\sigma_k = 1.0$, $\sigma_\epsilon = 1.2$, $C_1 = \max\{0.43, [\eta/(\eta+5)]\}$, $\eta = S\frac{k}{\epsilon}$. The constant C_μ is computed using the prescription of Shih et al. [25]. FLUENT commercial package is used for the simulations. The convective terms are discretized using a second-order upwind scheme whereas second-order central differencing is employed for the diffusive terms. The SIMPLEC algorithm is selected for the pressure–velocity coupling. The velocity profile and turbulence intensity level at the combustor inlet are obtained from the experimental study [11,24]. In the experimental setup, the flow exits to a plenum chamber and finally up an exhaust pipe to the atmosphere. There is no clear prescription for the boundary conditions at the exit of the combustor. Outflow boundary condition cannot be used because the combustor length is only $10H$, as opposed to $30H$, that is generally necessary for the flow to return to a fully developed state after separation. Consequently we employ a pressure outlet boundary condition at the combustor exit.

In wall bounded turbulent flows the near-wall modeling significantly impacts the fidelity of numerical solutions, inasmuch as walls are the main source of mean vorticity and turbulence. Therefore, an accurate representation of the flow near the wall often determines the successful prediction of the entire flow. In the context of RANS, traditionally there have been two approaches to modeling the near-wall region. In one approach the viscosity-affected inner region is not resolved, instead empirical laws known as wall functions are used to bridge the viscosity-affected region to the fully turbulent core. In another approach the turbulence models are modified to resolve the near-wall region all the way to the viscous sublayer. In this work we employ the second approach, wherein the whole domain is divided into a viscosity-affected region and a fully turbulent region. In the fully turbulent region high Reynolds number models such as realizable k–ϵ, RSM are solved, whereas in the near-wall region the one-equation model of Wolfstein [26] is considered.

Because the near-wall region is fully resolved a mesh with a $y^+ \approx 5$ at the wall adjacent cell is used for all the cases. Both orthogonal, structured mesh, and unstructured meshes are used depending on the complexity of the geometry. Grid independence of the numerical results is established through a systematic solution based grid adaption.

III. Results and Discussion

A. Turbulence Model Comparison

For the assessment of turbulence models we simulated the basic backward-facing step combustor, which will henceforth be referred to as the baseline case. A schematic of the baseline combustor is shown in Fig. 1. Figure 2 shows the axial velocity profiles at three different axial stations for the baseline case. The axial velocities have been normalized with the mean inlet velocity (U_0). The two-dimensional particle image velocimetry (PIV) technique was employed for data acquisition in the experiment. Mean and turbulent statistics were computed from ensembles of PIV realization. A minimum of 500 velocity fields were used to compute the statistics, resulting in precision errors of 2% of the inlet velocity. Further details on the uncertainty of the data can be found in [11]. We find that both the realizable k–ϵ and Reynolds stress models (RSM) compare well with the experimental data, especially in the shear layer, with RSM performing somewhat better near the reattachment point. However,

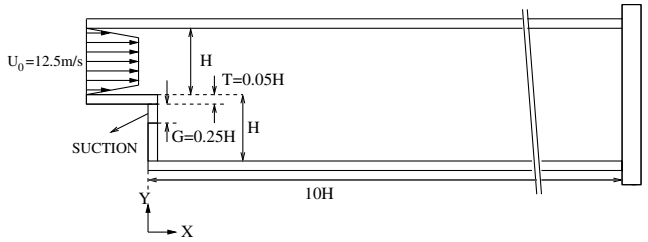

Fig. 1 Schematic of the baseline combustor (not to scale) considered in this study.

Reynolds stress models have a high relative computational overhead. Therefore, in all the subsequent simulations, the realizable k–ϵ model is used because of its good accuracy and low computational cost. The standard k–ϵ results are shown to fare poorly, especially away from the step.

The reattachment length L_r, predicted by the realizable k–ϵ model, has a value 8.5. The reattachment point is defined as the point on the bottom wall where the gradient of the axial velocity in the wall-normal direction is 0 [7]. Data for the reattachment length were not available from the experiment for comparison.

B. Effects of Countercurrent Shear

Having validated our modeling approach for the baseline case, we will now examine the effects of countercurrent shear on the flow characteristics for the basic step combustor of Fig. 1. We employ a suction level of 10.7% of the primary mass flow in our calculations, because most of the experimental data for comparisons were available for this case [24]. Figure 3 shows comparisons of the velocity profiles for numerical and experimental data for 10.7% counterflow at different axial locations. It is observed that the agreement with the experimental results is poor at $X/H = 7$. This is due to approximate modeling of the conditions at the combustor outlet. To investigate the influence of exit boundary condition, the length of the combustor was extended to $30H$ and outflow boundary conditions imposed. The results indicated the return to a fully developed turbulent channel flow state at about $X/H = 25$. We also observed that with the longer combustor the results improve only at locations considerably away from the step ($x/H > 5$). The flow field close to the step is largely unaffected by the change in length from $10H$ to $30H$. Moreover, because the primary objective of this research is a design study of a practical combustion system for ramjet applications, long combustors are not suitable candidates. Therefore we do not use it for any of our subsequent studies and restrict the length to $10H$ as in the laboratory model [11]. A comparison of Figs. 2 and 3 reveals that suction leads to rapid mixing and enhanced cross-stream transport of the streamwise momentum, resulting in much flatter velocity profiles. Increased mixing with countercurrent shear should lead to a better pattern factor, which is a measure of the spatial distribution of the mean temperature and velocity at the exit of the combustor. Figure 3a shows that the peak reverse velocity (located very close to the wall) is almost twice that of the baseline case. Figure 4 compares the cross-stream averaged turbulent kinetic energy for 0 and 6.5% suction cases. In the experiment, only fluctuations in streamwise and wall-normal directions are considered for kinetic energy calculation. The k–ϵ model implicitly assumes an

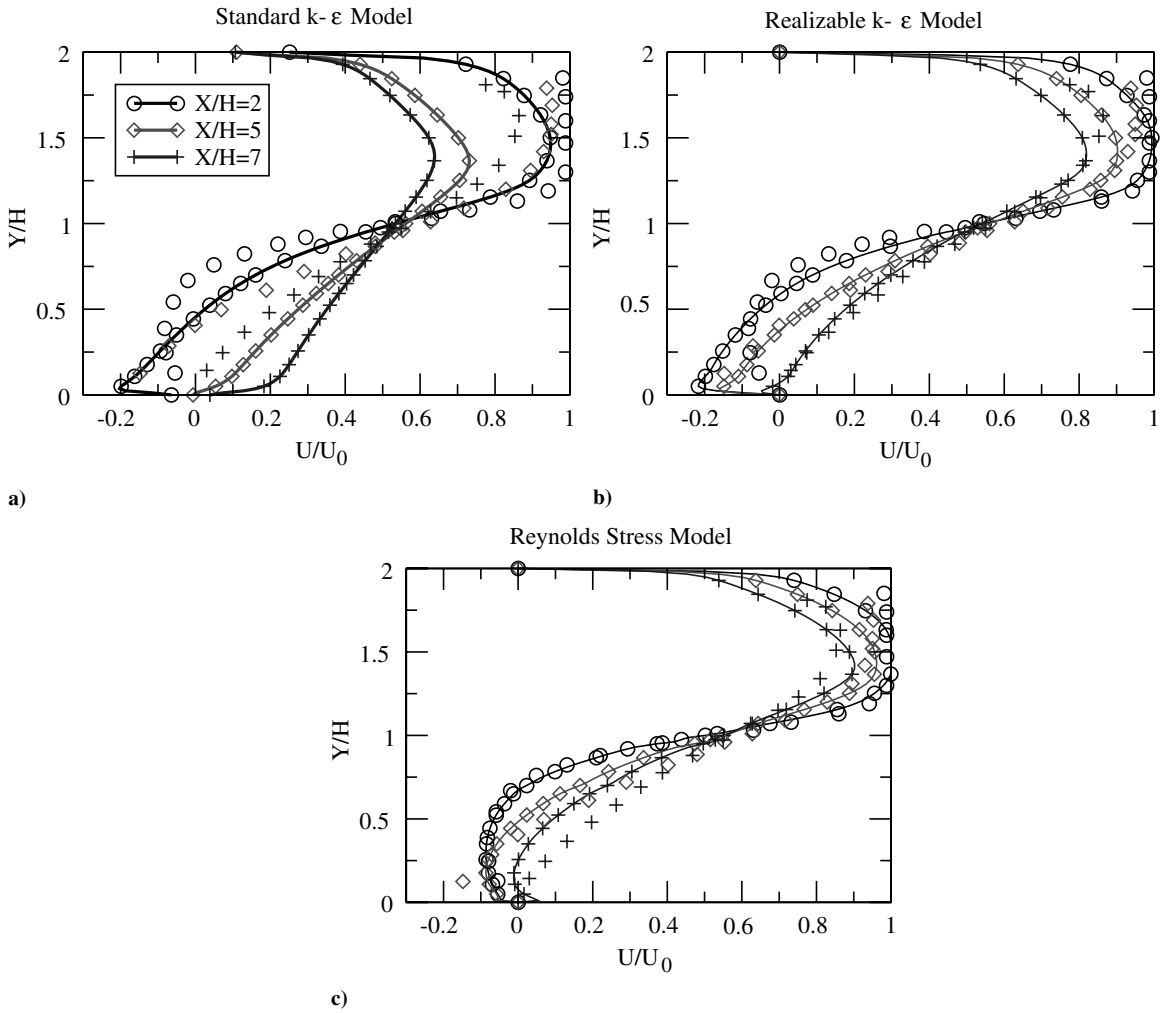

Fig. 2 Comparisons of turbulence models against experimental data for the baseline combustor without countercurrent shear. Continuous lines with markers indicate numerical model results, whereas markers without lines indicate experimental data.

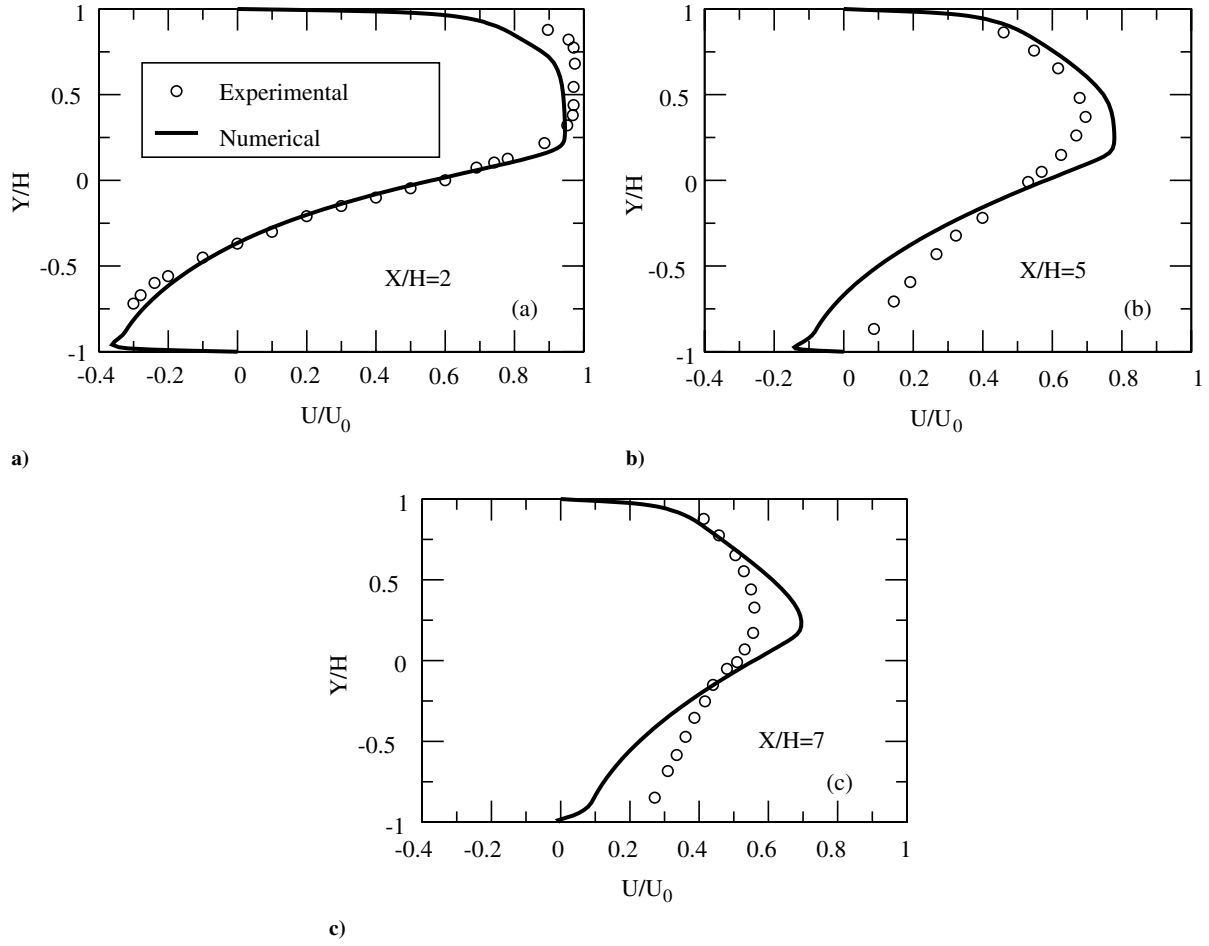

Fig. 3 Comparisons of axial velocity profiles at selected axial stations for the baseline combustor with 10.7% countercurrent shear flow.

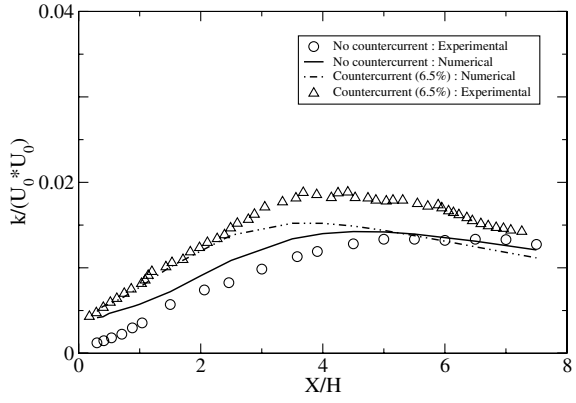

Fig. 4 Cross-stream averaged turbulent kinetic energy distributions for the baseline combustor.

isotropic turbulence (normal stresses are the same in all the three directions). Therefore, we consider only $\frac{2}{3}$ of the computed kinetic energy for comparison with the experimental data. The countercurrent case shows greater deviation especially in the downstream region. This can again be attributed to the approximate modeling of the suction and outlet boundary conditions.

Figure 5 shows the streamlines for cases without and with countercurrent. The most obvious change is the reduction of the streamwise length of the recirculation bubble. The movement of the recirculation bubble upstream, where the mean velocity gradients are higher leads to greater turbulence production. This shortening also leads to compact burning within the combustor. However, this can result in poor flame anchorage unless additional measures are taken. The wall pressure coefficient is an important parameter for engineering applications [21]. Figure 6 shows the pressure coefficient at the bottom wall of the baseline combustor for the 0 and 10.7% counterflow. Countercurrent flow leads to a greater pressure loss in the immediate vicinity of the step, due to the enhanced recirculation. However, it also results in a faster pressure recovery.

Analysis of turbulent quantities is essential because they directly impact the physics of the reacting flow within the combustor [27].

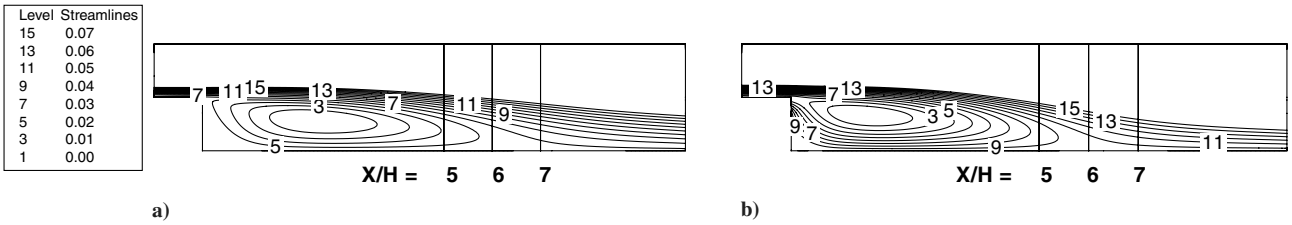

Fig. 5 Mean streamline contours a) 0% countercurrent flow with $L_r = 8.5H$ and b) 10.7% counterflow with $L_r = 7.5H$.

Table 1 Metric study for the baseline combustor

Cases	Compact, L_r	Turbulence	Strain rate	C_p	$C_f \times 10^4$
No countercurrent	No	$\propto U_0$	Limits operability	−0.356	9.36
Countercurrent	Yes	$\propto$ suction level	Lower strain rate	−0.466	13.5

Essentially there are two mechanisms for increased turbulence production in countercurrent combustor. The first one is the movement of the recirculation zone upstream as previously discussed. The second and equally important mechanism is the modification of the shear layer that originates at the separation point. The suction causes a strong countercurrent shear layer to develop near the trailing edge. The increased shear leads to higher turbulence production. Increased turbulence levels for the countercurrent case are observed in Fig. 7, where the turbulent kinetic energies for the baseline case with 0 and 10.7% countercurrent flow are compared. The figure also shows that the cross-stream width of the high turbulence region increases with the application of suction. A thicker region of high turbulence results in higher flame surface areas (more convoluted flames). Interestingly, turbulent kinetic energy near the end of the combustor is similar for both cases. This is also evident in Fig. 4 where the countercurrent case exhibits a decay of turbulence kinetic energy in the downstream region. This can be explained by the fact that suction increases the dissipation of turbulent kinetic energy in the upstream region where the fluctuations are high.

The other important flow feature that should be analyzed to determine the combustor performance under countercurrent shear is the strain rate. Strain rate influences combustion through flame stretch mechanisms. Excessive strain rate leads to local extinction of the flame. For the conventional dump combustor, turbulent kinetic energy and strain rate scale with U_0 [24]. Therefore, to increase the burning rate for the conventional dump combustor, one must increase the turbulence by increasing the inlet velocity, which also increases the strain rate. The analysis of the flow (not shown here) indicated that with countercurrent, the strain rate remains nominally invariant compared with the baseline case. Thus, one of the main advantages of countercurrent shear control is the increase of turbulence levels without the penalty of augmenting the strain rate to a great extent.

Table 1 summarizes the above findings. We conclude that a countercurrent combustor is characterized by higher turbulence levels, limited strain rate penalty, and compact burning. All of these translate to a more efficient energy conversion under reacting conditions. Unfortunately, comparisons of the drag coefficients reveals that both form and skin friction drags increase with the application of counterflow. C_P represents the average value along the step wall, whereas C_f is the average value along the bottom wall. Therefore, increasing drag penalty can potentially restrict the applicability of countercurrent combustors in actual ramjet systems. The drag penalty could be limited by employing lower levels of suction and reducing the combustor length.

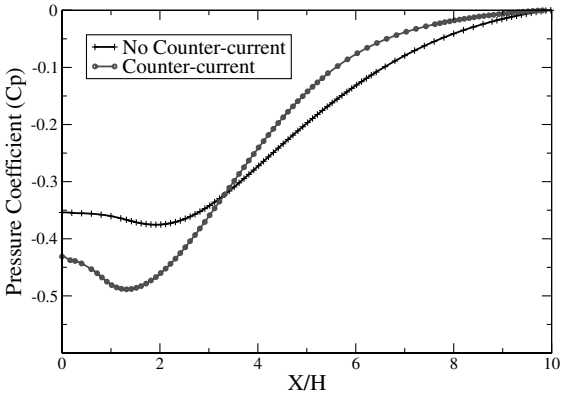

Fig. 6 Comparisons of C_p along the bottom wall of the baseline combustor for 0 and 10.7% countercurrent flow.

C. Step-Geometry Modification

Recent experimental investigation of countercurrent shear layers has demonstrated that turbulence can be increased by maintaining the negative velocity ratios over larger streamwise distances [28]. In a step-combustor configuration, negative velocity ratios can be readily achieved by implementing a step extension as illustrated in Fig. 8a. The step extension serves the dual purpose of providing a streamwise domain to enhance the countercurrent shear and as a bluff-body flame anchor. The success of any geometry in flame anchoring depends on the location and length of the recirculation zone. Figure 8a shows that two distinct recirculation regions occur within the combustor. Reacting flow experiments for this geometry show that the flame could not find a stable anchor in this configuration [28]. The upstream recirculation zone, being too compact, has an insufficient residence time for flame holding. For the downstream vortex, the burnt products failed to reach the fresh reactants due to the presence of a thick shear layer. A possible alternative to this step extension is to modify the extension surface to be sloped at different angles. The target design will enhance the counterflow effects by reducing the available cross-sectional area for the secondary stream, and by maintaining negative velocity ratios over large streamwise distances. At the same time, we want to ensure a suitable recirculation vortex for anchoring the flame.

In this section we perform a systematic study of the impact of altering the step extension geometry. It should be noted that geometry modification will influence even the base flow (no applied suction). To separate the effects of geometry change and suction, we simulate both the base and countercurrent flow for each configuration. Because countercurrent is associated with increased drag, we employ a moderate level of suction (5%). The reference axis for all the design cases is fixed at the tip of the trailing edge. Figure 8 depicts the streamlines for the step extension at angles of 0, 45, 60, and 70 deg. We observe that a secondary recirculation zone still exists for the 45 deg case in Fig. 8b. The secondary recirculation zone combines with the downstream bubble (main recirculation zone) to produce a single zone when the extension angle is increased to 60 deg, as shown in Fig. 8c. This single large vortex will provide greater residence time for the fresh reactants to achieve complete combustion. The streamline pattern for the 70 deg case shown in Fig. 8d is similar to the 60 deg case.

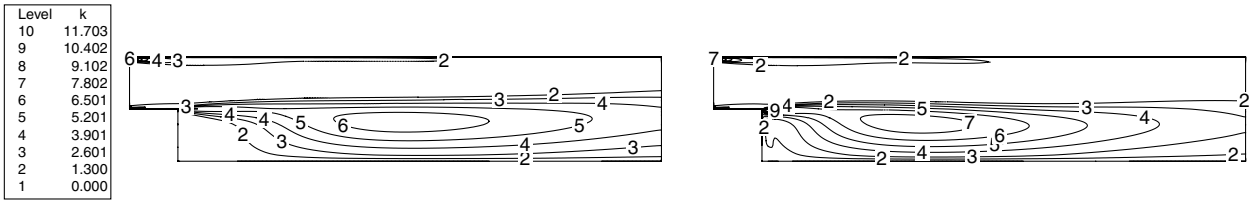

Fig. 7 Turbulent kinetic energy distributions for the baseline combustor a) 0% and b) 10.7% countercurrent flow.

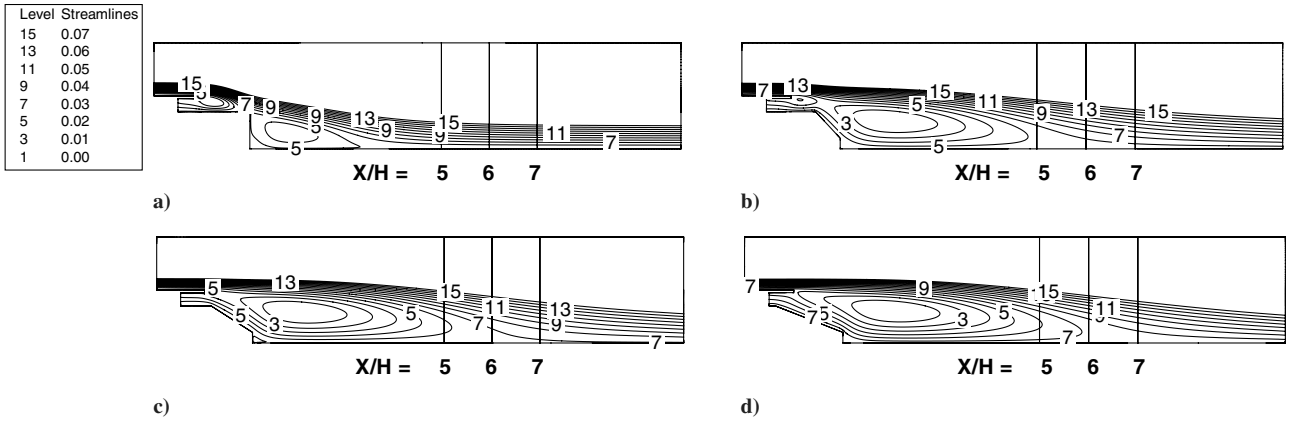

Fig. 8 Mean streamline contours for 5% countercurrent flow, showing the effects of geometry on the structure of the recirculation vortex a) 0 deg, b) 45 deg, c) 60 deg, and d) 70 deg step extension angles.

At the bulk Reynolds number of 13,600, which is considered in this study, the ratio of chemical time scale to turbulent (Kolmogorov) time scale, referred to as the Karlovitz number (Ka) is expected to be greater than unity. In this regime the premixed flame zone is modified by the turbulent motions [29]. The turbulent motions are often characterized by the root-mean-square (rms) fluctuating velocity which is the square root of the turbulent kinetic energy. Moreover, the global turbulent flame speed has been shown to be dependent on the rms velocity [30,31]. In the context of the current study, distribution of turbulent kinetic energy within the recirculation vortex determines the burning velocity of the fresh reactants. Thus, it is necessary to compare the turbulent kinetic energy profiles to judge the relative merit of each geometry. Cross-stream profiles of turbulent kinetic energy for the base flow (0% suction) is presented in Fig. 9. The 60 deg case has the highest turbulence level at each of the streamwise locations. Figure 10 reports the same quantity for the 5% countercurrent case. It is observed that suction has maximum impact on the profiles close to the step ($X/H = 1$ and $X/H = 2$) for all of the cases except 0 deg. Away from the step ($X/H = 3$ and $X/H = 4$), only the 70 deg case exhibits an appreciable increase in turbulence

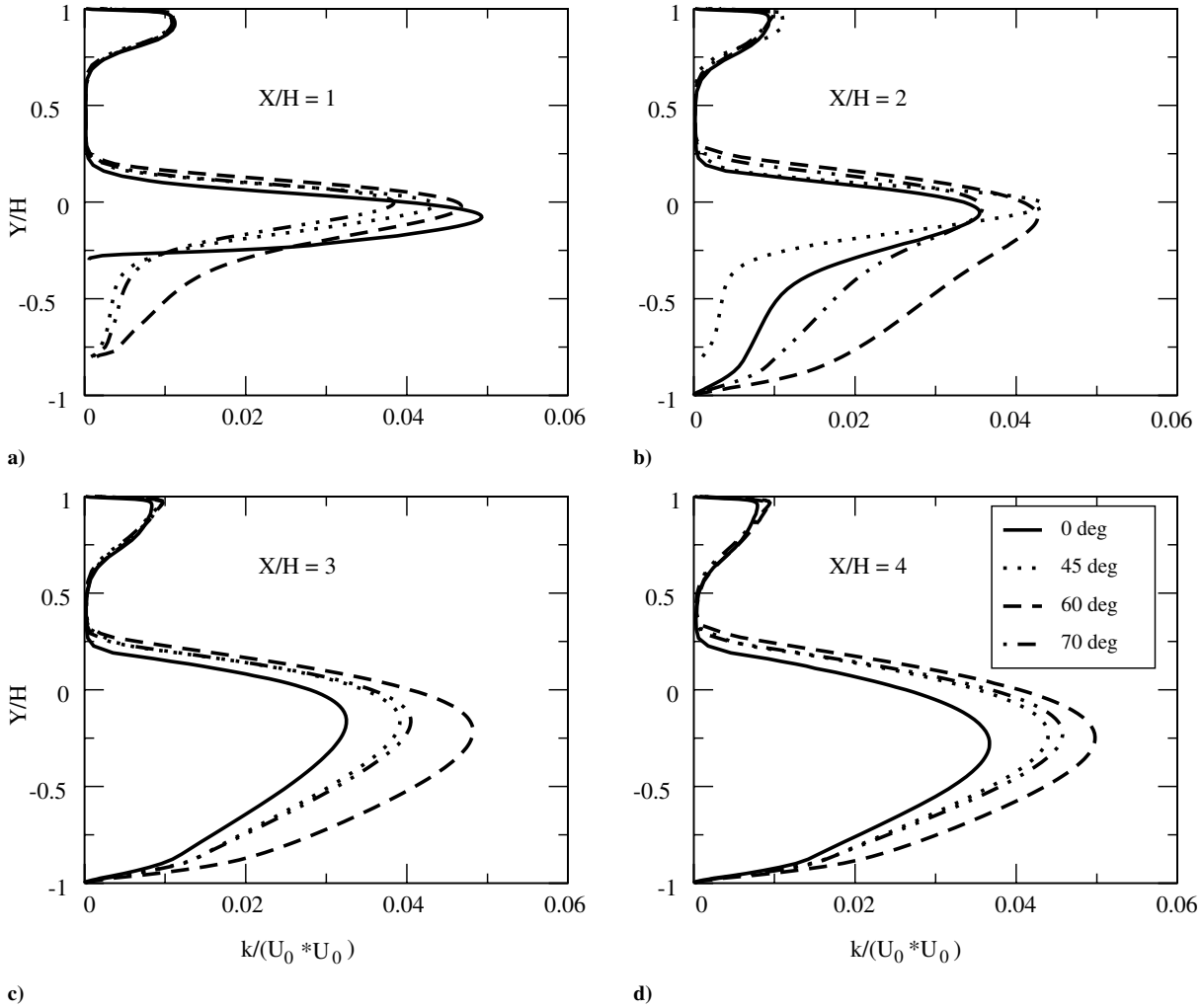

Fig. 9 Comparisons of turbulent kinetic energy profiles for 0% countercurrent flow within the recirculation vortex for different step extension geometries.

level. As discussed in the previous section, the enhanced recirculation and near field shear layer dynamics are the two mechanisms that alter the flow field in a countercurrent combustor. The region close to the dump plane (till about $X/H = 2$) behaves as counterflowing free shear layer. The dynamics therein are governed primarily by the velocity ratio U_2/U_1 [9], where U_1 and U_2 are the maximum velocities of the primary and secondary (counterflowing) streams, respectively, at a given axial station. Figures 11a and 11b show the above velocity ratios for different geometry cases. It is immediately observed that for all the configurations the peak velocity ratio is higher for the countercurrent case. The 0 deg configuration exhibits a sharp drop in the ratio to zero at about $X/H = 1$, which corresponds to the reattachment point of the upstream recirculation zone (Fig. 11b). The higher velocity ratio for the 60 deg design leads to more turbulence production and explains the higher levels of turbulent kinetic energy observed in Figs. 9 and 10 for this case. Figure 12 shows comparisons of strain rates. In general the tip of the splitter plate and boundary layer at the inlet duct can be identified as the highly strained regions in the flow. In turbulent shear flows, regions with high strain rate are also regions where dissipation of turbulent kinetic energy is large. Dissipation plays an important role in modeling of turbulent combustion [32]. The eddy dissipation concept set forth in [32] assumes that the chemical reaction occurs in regions where dissipation of turbulent energy takes place. Thus intense dissipation at the trailing edge of the splitter plate would help the flame to anchor at that location. Figure 12c shows that the 60 deg case produces the lowest strain rate in the shear layer.

Variations of the pressure coefficient along the bottom wall for different geometry configurations are presented in Fig. 13 for 0 and 5% cases. We observe that for the base flow, the 60 deg case has the fastest pressure recovery. The 45 and 70 deg cases have nearly identical recovery rates. As we move to the countercurrent cases, there is a substantial change in pressure loss along the bottom wall for the 70 deg case (Fig. 13b). The recovery rates are higher for the countercurrent flow for all the geometries. Tables 2 and 3 list C_p and C_f coefficients for different geometry cases. Again C_p is the average along the step wall. However, because the length of the step wall is different for each configuration, we consider the projected normal area of the step for drag coefficient calculation. Thus, for all the geometries we have the same surface area for pressure drag calculation. To estimate C_f, the areas considered are the horizontal projection of the step wall and the bottom wall. This again enables us to have the same surface area for all the cases and, consequently, make comparisons. As observed for the baseline combustor, countercurrent leads to an increase in both pressure and friction drag for the sloped step cases. For the countercurrent case (Table 3) the pressure drag increases with the increase in the step angle. The skin friction drag is found to be minimum for the 60 deg case.

Therefore, from the above analysis we conclude that the 60 deg step extension case is the best design candidate. It realizes the benefits of countercurrent shear most prominently and at the same time shows the promise of ensuring a suitable flame anchor. The aerodynamic drag penalty is also less for this configuration.

IV. Conclusions

A numerical study of the countercurrent step combustor with different step designs has been performed. Analysis of the flow

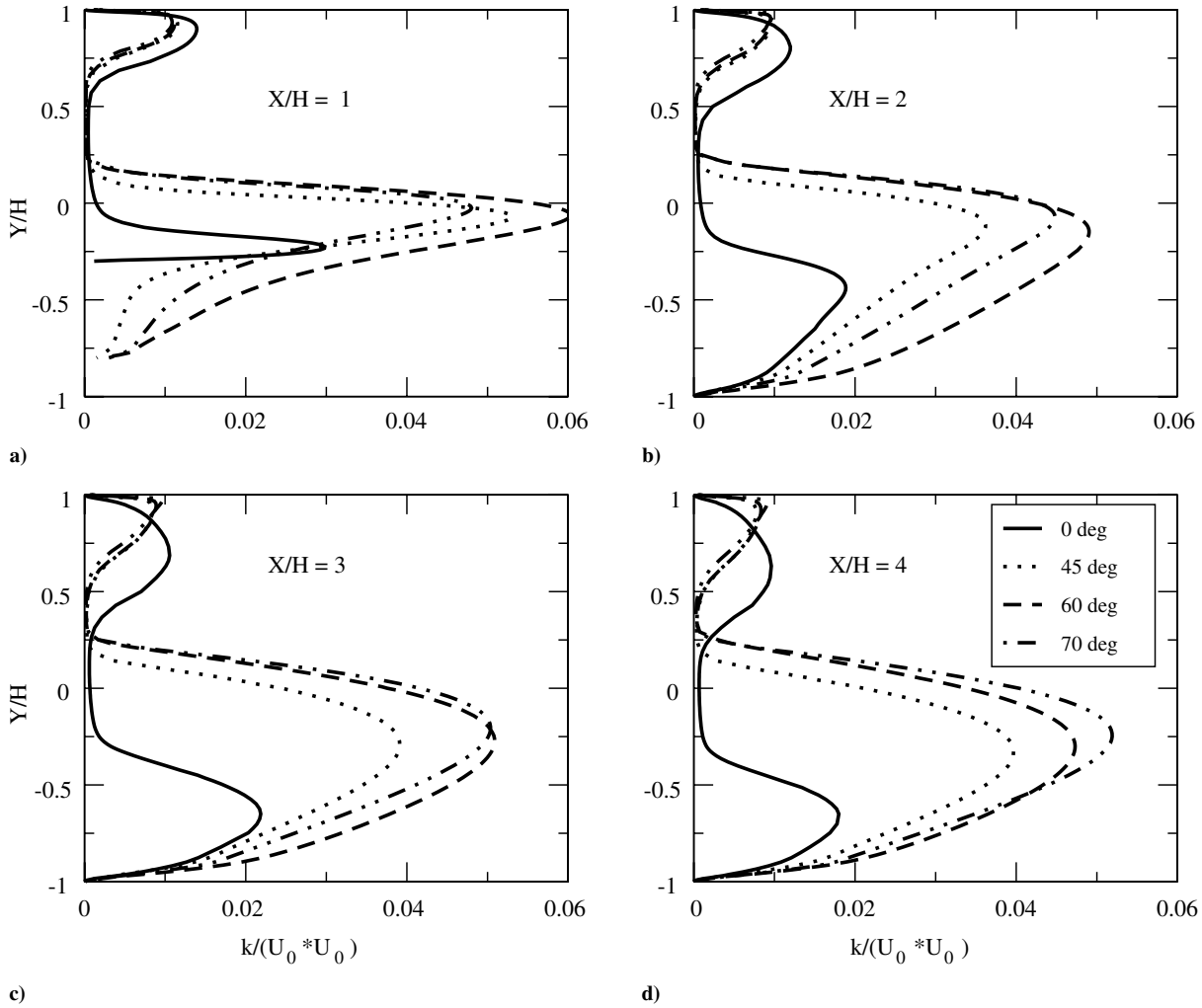

Fig. 10 Comparisons of turbulent kinetic energy profiles for 5% countercurrent flow within the recirculation vortex for different step extension geometries.

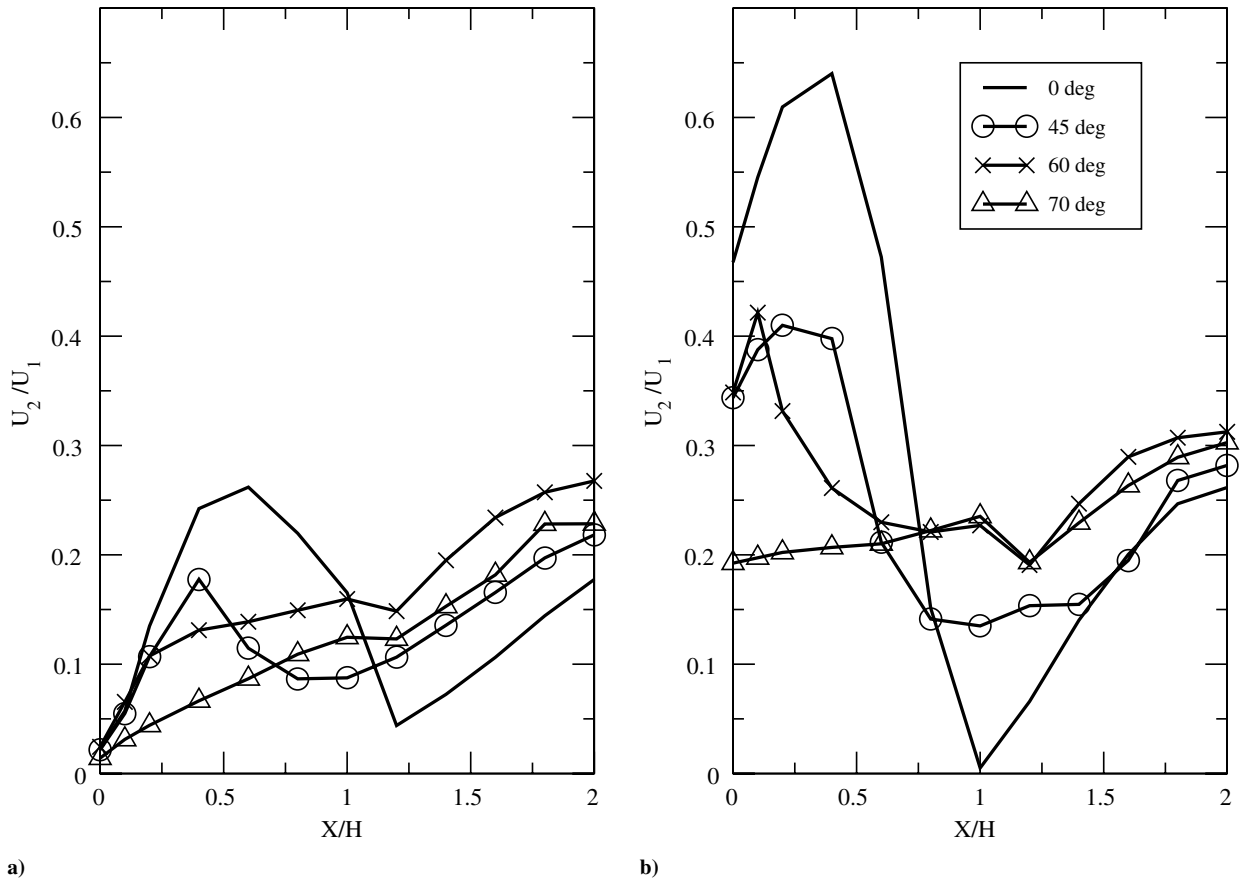

Fig. 11 Comparisons of streamwise velocity ratio for different step extension geometries a) 0% and b) 5% countercurrent flow.

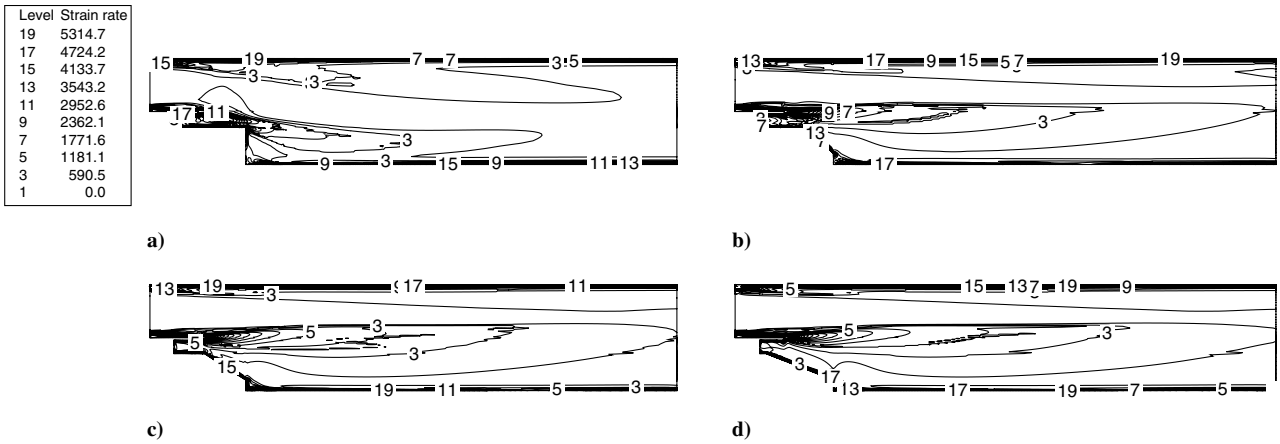

Fig. 12 Strain rate distributions for 5% countercurrent flow for different step extension angles a) 0 deg, b) 45 deg, c) 60 deg, and d) 70 deg.

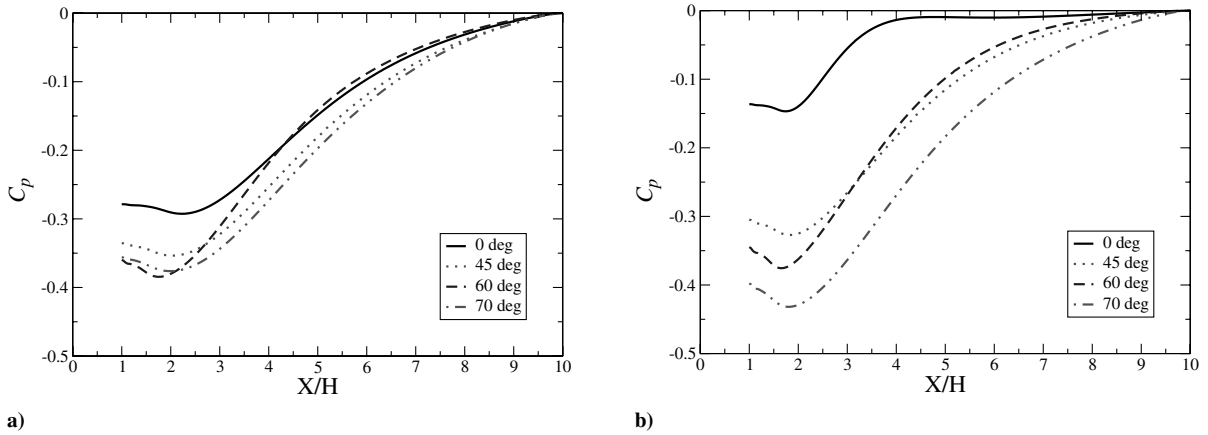

Fig. 13 Comparisons of C_p along the bottom wall for a) 0% and b) 5% countercurrent flow for different geometry configurations.

Table 2 Aerodynamic drag study for 0% counter-current flow

Cases	L_r	C_p	$C_f \times 10^4$
0 deg	8.1	−0.320	8.54
45 deg	8.5	−0.349	8.73
60 deg	8.6	−0.380	9.24
70 deg	8.7	−0.360	9.59

Table 3 Aerodynamic drag study for 5% counter-current flow

Cases	L_r	C_p	$C_f \times 10^3$
0 deg	3.75	−0.291	1.673
45 deg	7.15	−0.383	1.215
60 deg	8.0	−0.432	1.176
70 deg	8.5	−0.447	1.178

within traditional step combustor demonstrates that counterflow enhances turbulence production within the shear layer with a minimum strain rate penalty. Counterflow also leads to a compact recirculation zone and increases the cross-stream transport of streamwise momentum. Unfortunately, counterflow also increases the aerodynamic drag on the combustor. The effects of counterflow can be augmented by maintaining a large negative velocity ratio over a longer streamwise distance with a suitable extension of the step. Therefore, modifications to the geometry of the step were investigated to select the best design candidate for increasing counterflow effects with suitable flame anchoring capabilities. The 60 deg case promises to be the most suitable design in this aspect. Nevertheless, the dynamics of the flow could be quite different in reacting flow and this conclusion must be tested in the presence of combustion.

Acknowledgments

Support for this work was provided by the U.S. Office of Naval Research with G. D. Roy as the program officer. The authors would like to thank P. J. Strykowski for useful discussions on the physics of countercurrent shear.

References

[1] Adams, E. W., and Johnston, J. P., "Effects of the Separating Shear Layer on the Reattachment Flow Structure Part 1: Pressure and Turbulence Quantities," *Experiments in Fluids*, Vol. 6, No. 6, 1988, pp. 400–408.

[2] Adams, E. W., and Johnston, J. P., "Effects of the Separating Shear Layer on the Reattachment Flow Structure Part 2: Reattachment Length and Wall Shear Stress," *Experiments in Fluids*, Vol. 6, No. 7, 1988, pp. 493–499.

[3] Driver, D. M., and Seegmiller, H. L., "Features of a Reattaching Turbulent Shear Layer in Divergent Channel Flow," *AIAA Journal*, Vol. 23, No. 2, 1985, pp. 163–171.

[4] Spazinni, P. G., Iuso, G., Onorato, M., Zurlo, N., and Di Cicca, G. M., "Unsteady Behaviour of Back-Facing Step Flow," *Experiments in Fluids*, Vol. 30, No. 5, 2001, pp. 551–561.

[5] Armaly, B. F., Durst, F., Pereira, J. C. F., and Schonung, B., "Experimental and Theoretical Investigation of Backward-Facing Step Flow," *Journal of Fluid Mechanics*, Vol. 127, 1983, pp. 473–496.

[6] Neto, A. S., Grand, D., Metais, O., and Lesieur, M., "A Numerical Investigation of the Coherent Vortices in Turbulence Behind a Backward-Facing Step," *Journal of Fluid Mechanics*, Vol. 256, 1993, pp. 1–25.

[7] Hung, L., Moin, P., and Kim, J., "Direct Numerical Simulation of Turbulent Flow over a Backward-Facing Step," *Journal of Fluid Mechanics*, Vol. 330, 1997, pp. 349–374.

[8] Eaton, J. K., and Johnston, J. P., "A Review of Research on Subsonic Turbulent Flow Reattachment," *AIAA Journal*, Vol. 19, No. 9, 1981, pp. 1093–1100.

[9] Strykowski, P. J., Krothapalli, A., and Jendoubi, S., "The Effect of Counterflow on the Development of Compressible Shear Layer," *Journal of Fluid Mechanics*, Vol. 308, 1996, pp. 63–96.

[10] Strykowski, P. J., and Wilcoxon, R. K., "Mixing Enhancement due to Global Oscillations in Jets with Annular Counterflow," *AIAA Journal*, Vol. 31, No. 3, 1993, pp. 564–570.

[11] Forliti, D., and Strykowski, P. J., "Controlling Turbulence in a Rearward-Facing Step Combustor Using Countercurrent Shear," *Journal of Fluids Engineering*, Vol. 127, No. 3, 2005, pp. 438–448.

[12] Frolov, S. M., Basevich, V. Ya., and Belyaev, A. A., "Mechanism of Turbulent Flame Stabilization on a Bluff Body," *Chemical Physics Reports*, Vol. 18, No. 8, 2000, pp. 1495–1516.

[13] Mungal, M. G., and Dimotakis, P. E., "Mixing and Combustion with Low Heat Release in a Turbulent Shear Layer," *Journal of Fluid Mechanics*, Vol. 148, 1984, pp. 349–382.

[14] Hermanson, J. C., and Dimotakis, P. E., "Effect of Heat Release in a Turbulent, Reacting Shear Layer," *Journal of Fluid Mechanics*, Vol. 199, 1989, pp. 333–375.

[15] Pitz, R. W., and Daily, J. W., "Combustion in a Turbulent Mixing Layer Formed at a Rearward-Facing Step," *AIAA Journal*, Vol. 21, No. 11, 1983, pp. 1565–1570.

[16] McManus, K. R., Vandsburger, U., and Bowman, C. T., "Combustor Performance Enhancement Through Direction Shear Layer Excitation," *Combustion and Flame*, Vol. 82, No. 1, 1990, pp. 75–92.

[17] Gabruk, R. S., and Roe, L. A., "Velocity Characteristics of Reacting and Nonreacting Flows in a Dump Combustor," *Journal of Propulsion and Power*, Vol. 10, No. 2, 1994, pp. 148–154.

[18] Gao, Z., and Mashayek, F., "Stochastic Model for Non-Isothermal Droplet-Laden Turbulent Flows," *AIAA Journal*, Vol. 42, No. 2, 2004, p. 255.

[19] Gao, Z., Mashayek, F., Linck, M., and Gupta, A. K., "Experimental Results and Calculations of Two-Phase Flow in a Swirl Burner Under Isothermal Condition," AIAA Paper 2003-0336, 2003.

[20] Sengupta, K., Mashayek, F., and Gao, Z., "Numerical Study of Pulsed Injection for Control of Combustion," AIAA Paper 2005-0954, 2005.

[21] Thangam, S., and Speziale, C. G., "Turbulent Flow past a Backward-Facing Step: A Critical Evaluation of Two-Equation Models," *AIAA Journal*, Vol. 30, No. 5, pp. 1314–1320, 1992.

[22] Avva, R. K., Kline, S. J., and Ferziger, J. H., "Computation of Turbulent Flow over Backward Facing Step Using Zonal Modeling Approach," AIAA Paper 1988-0611, 1988.

[23] Benocci, C., and Skovgaard, M., "Prediction of Turbulent Flow over a Backward Facing Step," *Numerical Methods for Laminar and Turbulent Flows*, edited by C. Taylor, P. Gresho, R. L. Sani, and J. Hauser, Vol. 6, Pineridge, U.K., 1989, pp. 655–665.

[24] Forliti, D., Ph.D. Thesis, Department of Mechanical Engineering, Univ. of Minnesota, Minneapolis, MN, 2001.

[25] Shih, T. H., Liou, W. W., Shabbir, A., Yang, Z., and Zhu, J., "A New k–ϵ Eddy Viscoity Model for High Reynolds Number Turbulent Flows: Model Development and Validation," *Computer and Fluids*, Vol. 24, No. 3, 1995, pp. 227–238.

[26] Wolfstein, M., "The Velocity and Temperature Distribution of One-Dimensional Flow with Turbulence Augmentation and Pressure Gradient," *International Journal of Heat and Mass Transfer*, Vol. 12, 1969, pp. 301–318.

[27] Abdel-Gayed, R. G., Bradley, D., and Lawes, M., "Turbulent Burning Velocities: A General Correlation in Terms of Straining Rates," *Proceedings of the Royal Society of London A*, Vol. 414, No. 1847, 1987, pp. 389–413.

[28] Behrens, A. A., Anderson, M. J., Forliti, D. J., and Strykowski, P. J., "Role of Enhanced Recirculation in Controlling Turbulent Combustion and Flame Anchoring in a Step Combustor," *Proceedings of 17th ONR Propulsion Meeting*, MIT Press, Cambridge, MA, 2004, pp. 27–32.

[29] Veynante, D., and Vervisch, L., "Turbulent Combustion Modeling," *Progress in Energy and Combustion Science*, Vol. 28, 2002, pp. 193–266.

[30] Abdel-Gayed, R. G., and Bradley, D., and Hamid, M. N., "Lewis Number Effects on Turbulent Burning Velocity," *20th International Symposium on Combustion*, Combustion Institute, Pittsburgh, PA, 1984, pp. 505–512.

[31] Abdel-Gayed, R. G., Bradley, D., and Lung, F. K. K., "Combustion Regimes and the Straining of Turbulent Premixed Flames," *Combustion and Flame*, Vol. 76, No. 2, pp. 213–218, 1989.

[32] Gran, I. R., and Magnussen, B. F., "A Numerical Study of a Bluff-Body Stabilized Diffusion Flame Part 2: Influence of Combustion Modeling and Finite-Rate Chemistry," *Combustion Science and Technology*, Vol. 119, No. 1–6, 1996, pp. 191–217.

T. Jackson
Associate Editor